

Chemical composition and discharge characteristics of γ -MnO₂ prepared using manganese ore

H. Malankar · S. S. Umare · K. Singh · M. Sharma

Received: 12 September 2008 / Revised: 11 January 2009 / Accepted: 14 January 2009 / Published online: 28 January 2009
© Springer-Verlag 2009

Abstract γ -MnO₂, synthesized chemically from local manganese ore, was subjected to physicochemical studies. X-ray diffraction, Fourier transform infrared spectroscopy, surface area measurement, thermogravimetry/differential thermal analysis, scanning electron microscopy, and chemical analyses were used to determine the structural and chemical disorder present in the samples. The electrochemical activity in alkaline medium was evaluated by recording discharge profile at constant current and constant load condition. The charge–discharge profile in 9 M KOH was studied by cyclic voltammetry. The samples were found to be “type III” γ -MnO₂ with high degree of microtwinning defect (T_w). The De Wolff disorder was in the range $0.21 < P_r < 0.32$. Thermal studies showed weight loss due to the loss of structural water and formation of lower manganese oxides. Mn⁴⁺ vacancy, calculated on the basis of cation vacancy model, was in range $0.06 < x < 0.1$. The discharge in alkaline medium was accompanied by homogeneous solid-state proton diffusion in MnO₂ lattice. The energy density is explained as a function of proton transfer rate (P_t) during the discharge.

Keywords γ -MnO₂ · Manganese ore · De Wolff disorder · Cation vacancy model · Electrochemical behavior

Introduction

Synthetic manganese dioxides found application in different production fields [1]. In a major nonmetallurgical application, manganese dioxide (MnO₂) material has been widely used as a positive electrode for primary and secondary batteries as it is a low cost and environmentally benign material [2]. Natural manganese dioxide (NMD) is consumed in combination with other varieties of MnO₂ (such as chemical manganese dioxide [CMD], activated manganese dioxide [AMD], and electrolytic manganese dioxide [EMD]) for the manufacture of dry cells owing to its cost-effectiveness [3]. The rapidly growing demand for manganese has made it increasingly important to develop processes for economical recovery of manganese from low-grade manganese ores and other secondary sources [4]. Exploiting low-grade ores in an economic procedure is suitable for obtaining better quality manganese dioxide [5]. The traditional methods of ore enrichment consist of reducing the pyrolusite in the first stage to manganese (II) oxide followed by leaching with sulfuric acid and then a chemical or electrochemical oxidation [5–8]. Activation with mineral acids and doping are two other major techniques that are employed for the enrichment.

Activation of manganese ore, which results in the formation of active cathode material, involves disproportionation of the ore with dilute mineral acids. Various physicochemical principles involved in the activation of natural manganese ore [8] and electrochemical behavior of activated manganese ore have been reported [9]. The MnO₂ synthesized using this technique, however, shows the

H. Malankar (✉) · S. S. Umare
Department of Chemistry,
Visvesvaraya National Institute of Technology,
Nagpur 440011, India
e-mail: hemant.malankar@gmail.com

K. Singh
Sant Gadge Baba Amaravati University,
Amaravati 444602, India

M. Sharma
Department of Electronics, SFS College,
Nagpur 440 006, India

presence of iron as an impurity that is undesirable for battery-grade manganese dioxide. Use of doped NMD as a cathode material has been reported [3]. In more recent literature, synthesis of γ - MnO_2 from low-grade manganese ore [10] and its role as a cathode in alkaline Zn- MnO_2 system has been studied [10, 11].

The present work is aimed to characterize γ - MnO_2 obtained from manganese ore as cathode vs Zn anode in alkaline Zn- MnO_2 system. The synthesis procedure involves removal of impurities such as iron and silica that are present in the starting material. The obtained product has been thoroughly characterized by chemical analysis. A structural description of X-ray diffraction (XRD) pattern based on two structural defects, De Wolff disorder and microtwinning, is presented. Physical properties and chemical composition of prepared MnO_2 samples are explained on the basis Ruetschi's Mn^{4+} cation vacancy model. In the application part, electrochemical activity and cyclic voltammetry of prepared γ - MnO_2 samples in 9 M KOH are discussed.

Experimental

Methods

For the present study, manganese ore from Kanhan mines, Nagpur with composition MnO_2 74%, Mn 48%, SiO_2 8%, and Fe 10% was provided by M/s. Manmohan International, Nagpur. The ore with 3–20 mm size was charged in fixed bed chamber furnace where in situ gas reduction of MnO_2 with carbon was carried out at ~ 600 °C. During this stage, the Mn ore is converted into reactive Mn(II) form, which was used for the synthesis. The above process was carried out at M/s. Manmohan International, Nagpur.

Other chemicals used, viz., liquor ammonia (30%), HNO_3 , HCl, H_2SO_4 , ethylenediaminetetraacetic acid (EDTA), oxalic acid, and KOH, were of Merck (AR) grade. Thymolphthalein complexone graphite was of Sigma-Aldrich (AR) grade.

Synthesis

One hundred grams of the above material was leached with 400 mL of 70% H_2SO_4 at 90 °C for 30 min. The reaction mixture was filtered through Buckner funnel to remove insoluble impurities like silica. The MnSO_4 solution prepared by leaching with hot H_2SO_4 was purified using the following steps [12]: (1) oxidation of Fe^{2+} to Fe^{3+} ion by addition of MnO_2 powder to the solution at 80–90 °C while bubbling air through the solution; (2) neutralization of the solution by CaCO_3 in order to precipitate $\text{Fe}(\text{OH})_3$ from the solution; (3) filtration of the precipitate. The filtrate was allowed to attain

room temperature (RT, 27 °C). Liquor ammonia was added to this filtrate at pH 10 to precipitate manganese hydroxide. The $\text{Mn}(\text{OH})_2$ precipitate was filtered and washed with distilled water till the filtrate showed pH 7. The obtained precipitate was suspended in 200 mL deionized water and air was passed through the suspension for 72 h at the rate of 4 L/min at different temperatures, viz., RT (27 °C), 40 °C, 60 °C, and 80 °C. It was then further subjected to disproportionation in concentrated nitric acid. The MnO_2 obtained by air oxidation at different temperature(s), i.e., RT, 40 °C, 60 °C, and 80 °C are, henceforth, designated by the acronyms ORE-RT, ORE-40, ORE-60, and ORE-80, respectively. The samples were air-dried in an oven at 110 °C for 1 h and cooled in a desiccator.

Chemical analysis

Total manganese content (%Mn) in the synthesized MnO_2 was estimated by titration against EDTA [13]. Available oxygen in terms of % MnO_2 was determined by redox titration against KMnO_4 [14]. In order to check the impurities in the final product, ORE-RT was analyzed by atomic absorption spectroscopy (AAS). The standard stock solutions containing 1,000 $\mu\text{g}/\text{cm}^3$ of the elements Fe, Ni, Co, and Cu were prepared, and then the working standard solutions were prepared by suitable dilution of these stock solutions. Surface area measurement was carried out using nitrogen adsorption with the six-point Brunauer, Emmett, and Teller (BET) method on the ASAP 2010 (Accelerated Surface Area and Porosity Measurement System) of Micromeritics USA.

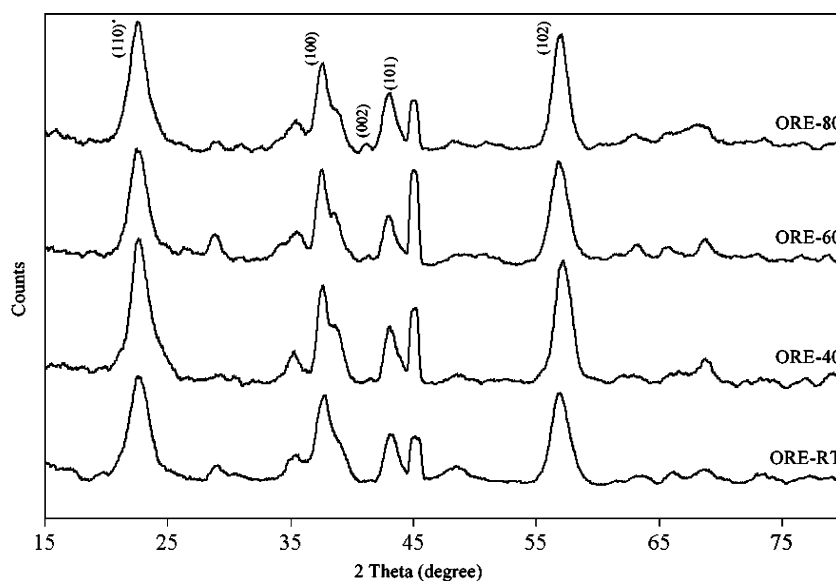
Structure and morphology

The XRD patterns were recorded on PANalytical X-ray diffractometer (Philips, Holland) using $\text{Cu K}\alpha$ radiation ($\lambda = 1.5418$ Å). The scans were recorded in 2θ range 15–80° with a step size of 0.02° and count size of 0.5° 2θ /min. Fourier transform infrared spectroscopy (FTIR) for the prepared MnO_2 samples were recorded on Shimadzu spectrophotometer in the frequency range of 400–4,600 cm^{-1} . The surface morphology of synthesized samples was determined using a scanning electron microscope (JEOL: JSM-6380A) equipped with an electron probe analyzer system (accelerating voltage 30 kV). The sample was coated with platinum sputtering in order to have good conductivity.

Thermal analysis

Differential thermal analysis (DTA) and thermogravimetry (TG) of the samples was carried out using Perkin Elmer (Diamond Module) instrument in argon atmosphere in the temperature range 30 to 1,200 °C at the heating rate of 5 °C/min.

Fig. 1 XRD pattern of MnO₂ samples prepared at different temperatures



Electrochemical activity

The electrochemical activity of the prepared samples was evaluated by recording discharge profile in 9 M KOH electrolyte solution at constant current of 1 mA/0.1 g and constant resistance of 100 Ω /0.5 g at 27 °C (RT). The experimental cell consisted of a zinc anode strip (50 \times 10 mm) and the cathode consisted of 0.1 g of the synthesized MnO₂ dispersed in 0.4 g of graphite powder wetted with 0.5 mL of electrolyte and carboxymethyl cellulose binder. For discharge profile at 100 Ω , cathode mixture consisted of 0.5 g MnO₂ dispersed in 0.5 g graphite powder. The cathodic ingredients were pressed in a cylindrical Teflon container (50 mm height and 20 mm diameter) with a spiral platinum wire at the bottom for electrical contact at a pressure of 100 kg cm⁻². A circular, perforated, Teflon disc was placed over the compressed mixture for ionic transfer and to avoid diffusion of cathodic mixture into the

electrolyte media. The cell was activated with 10 mL of electrolyte. The total cell assembly was allowed to equilibrate for 1 h at its open-circuit potential before measurement of continuous discharge till cutoff voltage 0.7 V (for 1 mA) and 0.6 V (for 100 Ω), respectively.

Cyclic voltammetry

Cyclic voltammetry of ORE-RT was carried out with a three-electrode setup comprising the MnO₂-containing platinum working electrode and a Hg/HgO/9 M KOH reference electrode and platinum wire auxiliary electrodes. The electrochemical cell was controlled and data were collected by Autolab Potentiostat–Galvanostat using the cyclic voltammetry software option. Voltammogram were recorded between 400 and –800 mV at 2 mV/s in 9 M KOH solution. MnO₂-containing working electrode was prepared according to the procedure described elsewhere [15].

Table 1 Lattice, P_r , and T_w parameters obtained from XRD measurements

Sample code	Crystal phase/type ^a	a (Å)	c (Å)	Cell volume (cm ³)	T_w (%)	P_r
ORE-RT	γ /III	2.798 (± 0.007)	4.449 (± 0.014)	30.155 (± 0.166)	>70	0.26
ORE-40	γ /III	2.797 (± 0.010)	4.462 (± 0.056)	30.234 (± 0.378)	>70	0.23
ORE-60	γ /III	2.800 (± 0.016)	4.447 (± 0.029)	30.205 (± 0.360)	>70	0.21
ORE-80	γ /III	2.797 (± 0.006)	4.440 (± 0.014)	30.074 (± 0.158)	>70	0.32
Ref. [17]	γ /III	2.78	4.43	–	>70	–
Ref. [18]	γ	2.80	4.45	30.210	–	–
Ref. [10] EMD	γ /III	2.774	4.419	29.443	>70	0.37
Ref. [10] EMD	γ /III	2.775	4.424	29.510	>70	0.31
Ref. [10] CMD	γ /III	2.778	4.463	29.827	>70	0.44

Data are presented as the mean (\pm SE; standard error at the 95% level of confidence)

^a According to the method suggested by Chabre and Pannetier [17]

Results and discussion

X-ray diffraction analysis

Figure 1 presents the XRD spectra of the prepared manganese dioxides. A typical γ - MnO_2 spectrum based on the presence of mere five to six broadened peaks indicates that the samples contain many structural defects. These type of patterns were referred to as “lower structure manganese dioxides” by Malpas and Tye [16]. Based on the orthorhombic symmetry, the XRD patterns show merging of lines 221 and 240 or 002 and 061, which, in turn, suggests that these samples contain heavy microtwinning defect ($T_w > 70\%$). Such patterns can no longer be indexed with an orthorhombic unit cell. Ignoring the presence of the first line, i.e., 110, in orthorhombic Pbnm indexing (peak 110* in Fig. 1), they are indexed with a hexagonal cell with parameters $a_h = 2.78 \text{ \AA}$ and $c_h = 4.43 \text{ \AA}$ [17]. This type of MnO_2 with hexagonal symmetry was originally proposed by De Wolff et al. [18] for EMD samples called as ϵ - MnO_2 . Recent reports [19, 20] describe ϵ - MnO_2 as a MnO_2 polymorph with hexagonal symmetry with unit cells $a_h = 2.80 \text{ \AA}$ and $c_h = 4.45 \text{ \AA}$ and space group $P6_3/mmc$ (JCPDS card no. 30-0820). The structure is the same as that of NiAs-type containing 50% randomly spaced Mn^{4+} cation vacancies of the octahedral positions of the hexagonal close-packed (hcp) oxygen sublattice.

Chabre et al. [17] have classified these types of XRD patterns as extensively twinned “type III” γ - MnO_2 samples. For such samples, the amount of De Wolff disorder (P_r) is estimated from the displacement of peak 110 from the orthorhombic position after correction for the shift due to microtwinning. The P_r values for the prepared samples were in the range $0.21 < P_r < 0.32$ (Table 1). The lattice parameters (Table 1) calculated according to hexagonal symmetry are in good agreement with the values reported earlier [10, 17, 18].

FTIR analysis

Figure 2 presents the FTIR spectra of the synthesized manganese dioxides. The absorption band at $\sim 3,600 \text{ cm}^{-1}$ represents O–H stretching vibration, whereas the strong absorption band at $\sim 1,620 \text{ cm}^{-1}$ corresponding to O–H bending vibration is associated with the water of crystallization [21]. The broad absorption band in the region 600 to 400 cm^{-1} suggests the formation of γ - MnO_2 . The absorption band at $1,100 \text{ cm}^{-1}$ is attributed to the presence of hydrogen bonding [22] and/or MnO_2 stretching mode [23]. The OH^- groups as well as H_2O molecules, associated as bound water, within the crystal structure [22, 23] influences the electrochemical activity of MnO_2 [24].

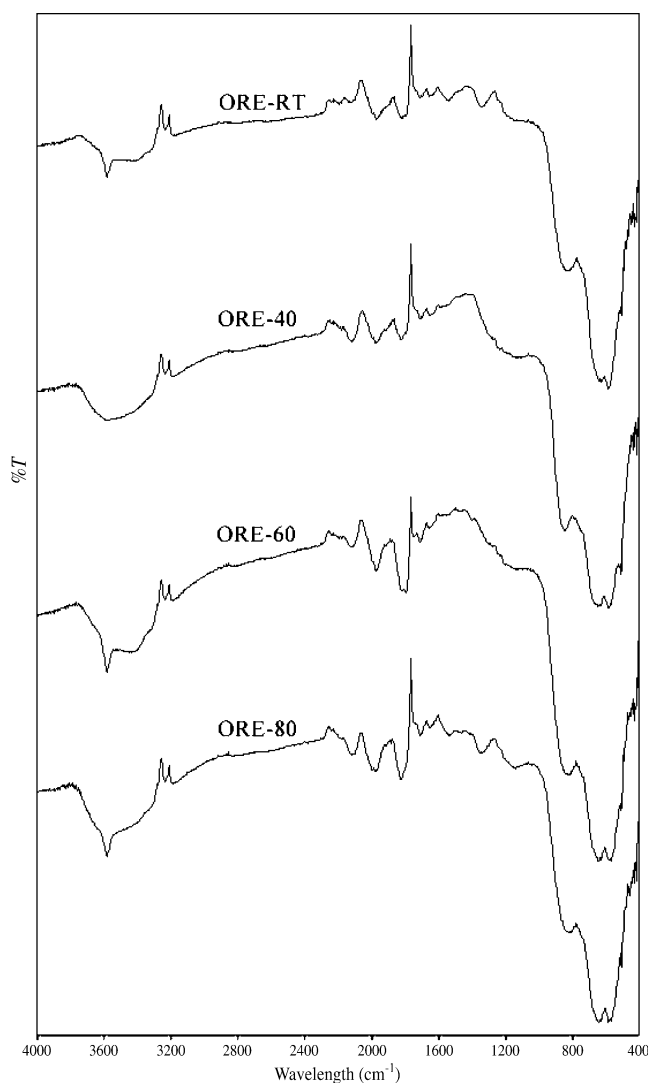


Fig. 2 FTIR spectra of MnO_2 samples prepared at different temperatures

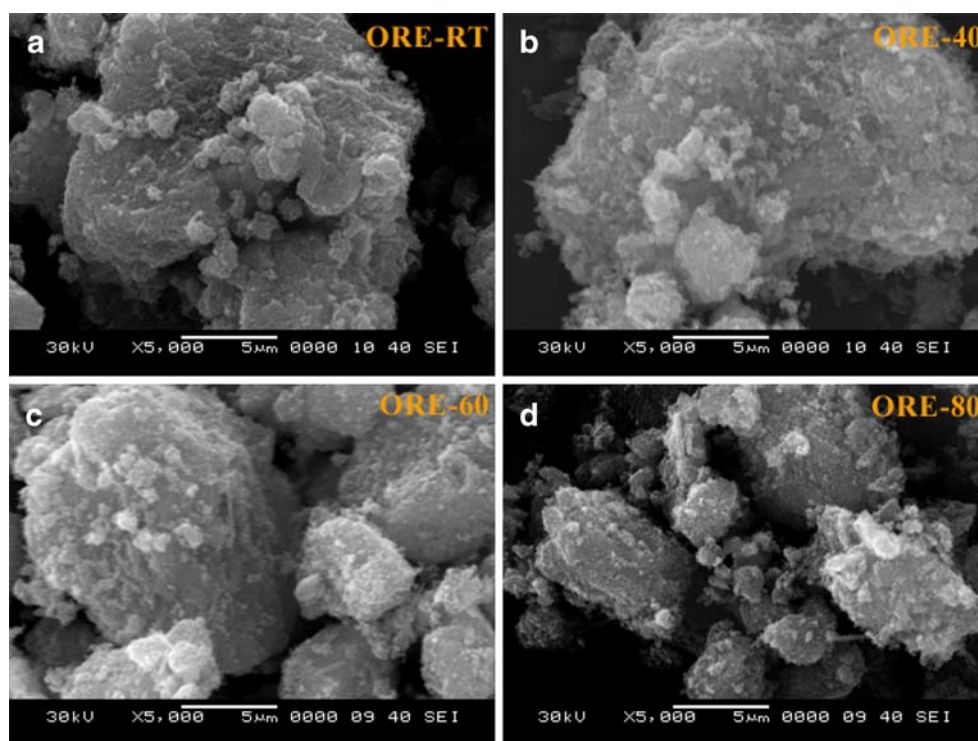
SEM

The scanning electron microscopy (SEM) images of synthesized MnO_2 samples are shown in Fig. 3. The particles are irregular and random in shape. Samples exhibit porous morphology with agglomerating tendency forming a cluster.

Thermal analysis

The TG thermograms of the prepared samples (Fig. 4) showed gradual weight loss due to the loss of adsorbed and structural water and loss of oxygen followed by the formation of lower oxides, viz., Mn_2O_3 and Mn_3O_4 . The weight loss up to a temperature of $110 \text{ }^\circ\text{C}$ is due to the removal of physically adsorbed moisture. The weight loss from 110 to $300 \text{ }^\circ\text{C}$ is due to the removal of chemically bound water associated with γ - MnO_2 . Three different types of water associated with

Fig. 3 SEM images of prepared MnO₂: **a** ORE-RT; **b** ORE-40; **c** ORE-60; and **d** ORE-80



γ -MnO₂ have been reported [25]. Type I water corresponding to physisorbed molecular water is removed below 110 °C. Type II water, which is made up of dissociatively chemisorbed water and strongly bound micropore water, is removed below 270 °C. Type III water is present as hydroxyl groups in the interior of the lattice and is removed around 300 °C. This is followed by the weight loss in the temperature range 400–600 and 600–900 °C, which indicates thermal decomposition resulting in the formation of Mn₂O₃ and Mn₃O₄, respectively [26–28].

Figure 5 presents the DTA thermograms of the prepared samples. A broad endotherm up to 300 °C is due to the continuous removal of type I, type II, and type III water. The

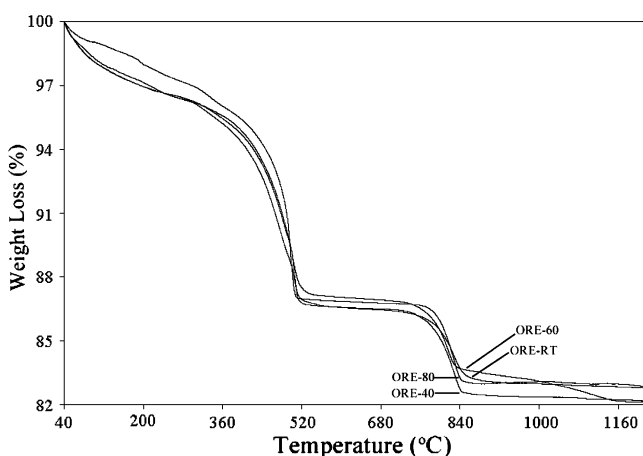
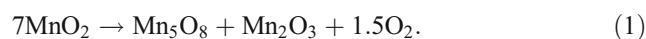
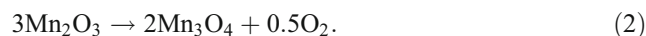


Fig. 4 TG thermograms of MnO₂ samples prepared at different temperatures

DTA thermogram of ORE-40 and ORE-80 are similar, whereas that of ORE-RT and ORE-60 are similar. While thermal decomposition reactions MnO₂→Mn₂O₃ and Mn₂O₃→Mn₃O₄ for ORE-40 take place at 501 and 824 °C, respectively, that for ORE-80 takes place at 494 and 825 °C, respectively. During the decomposition of ORE-RT and ORE-60, the partial reduction of MnO₂ to the intermediate phase Mn₅O₈ was observed in significant proportions between the temperatures 450 and 500 °C. The Mn₂O₃ phase was also observed between 450 and 550 °C. The first peak in the thermogram at 472 °C for ORE-RT and 477 °C for ORE-60 corresponds to the decomposition of MnO₂ to Mn₅O₈ and Mn₂O₃ [29] according to the reaction:



Further heating results in the decomposition of Mn₂O₃ to Mn₃O₄ at ~800 °C, according to the reaction:



Both reactions 1 and 2 involve the loss of oxygen during the formation of lower oxides. The rate of removal of oxygen from the reaction site and physical factors such as particle size, crystallite size, porosity, and crystal structure can result in the variation of the decomposition temperatures [29–31].

Chemical composition and formulae

ORE-RT tested by AAS showed the presence of the following impurities Fe=900 ppm, Ni=7 ppm, Co=

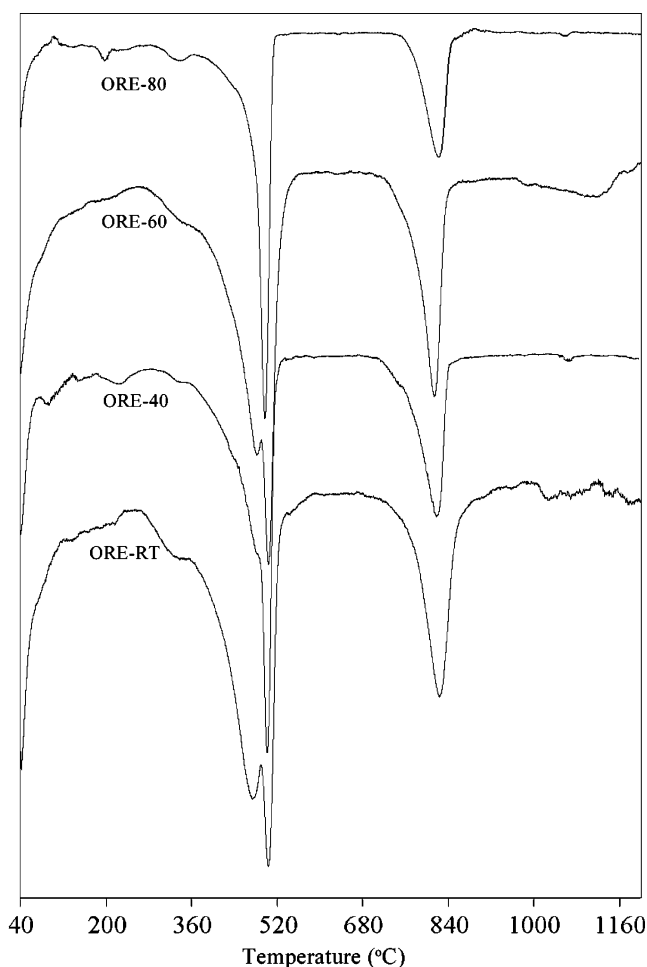


Fig. 5 DTA thermogram of MnO_2 samples prepared at different temperatures

8 ppm, and $\text{Cu}=17$ ppm. The chemical analysis data are presented in Table 2. The high values of available oxygen ($\%\text{MnO}_2$) and BET surface area indicate good catalytic activity as well as suitability for cathode material. Based on the chemical composition data, the formulae are expressed in the format proposed by Brenet [32], which is as follows:



where m denotes neutral water molecules and n is the degree of oxidation.

The n and m are calculated using following relation:

$$n = (3 + z)/2 \quad (3)$$

where z in MnO_{1+z} is the ratio of reducible Mn to the total Mn and is calculated using the relation:

$$z = (0.632 \times \%\text{MnO}_2)/\%\text{Mn}. \quad (4)$$

The number of neutral water molecules m in the crystal lattice is calculated using the relation:

$$m = (91w + 2n(900 - w) - 3,600)/18(100 - w) \quad (5)$$

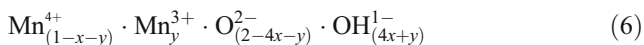
Table 2 Chemical composition, reactivity and formulae of prepared manganese dioxides

Sample code	MnO_2 (%)	Mn (%)	z in MnO_{1+z}	Combined water (w) (%)	Neutral water molecules (m)	Degree of oxidation (n)	BET surface area (m^2/g)	Formula $(\text{MnO}_2)_{(2n-3)} \cdot (\text{MnOOH})_{(4-2n)} \cdot m\text{H}_2\text{O}$
ORE-RT	93.92 (± 0.82)	61.16 (± 0.35)	0.970 (± 0.004)	4.28 (± 0.01)	0.200 (± 0.002)	1.985 (± 0.001)	120.30 (± 2.0)	$(\text{MnO}_2)_{0.9705} \cdot (\text{MnOOH})_{0.0294} \cdot 0.200\text{H}_2\text{O}$
ORE-40	91.62 (± 0.50)	62.61 (± 0.36)	0.925 (± 0.007)	3.41 (± 0.20)	0.132 (± 0.007)	1.962 (± 0.003)	78.55 (± 2.0)	$(\text{MnO}_2)_{0.9249} \cdot (\text{MnOOH})_{0.0750} \cdot 0.132\text{H}_2\text{O}$
ORE-60	89.42 (± 0.51)	60.17 (± 0.33)	0.939 (± 0.002)	4.37 (± 0.15)	0.189 (± 0.008)	1.969 (± 0.001)	104.32 (± 2.0)	$(\text{MnO}_2)_{0.9392} \cdot (\text{MnOOH})_{0.0607} \cdot 0.189\text{H}_2\text{O}$
ORE-80	88.01 (± 0.51)	59.40 (± 0.35)	0.936 (± 0.002)	4.73 (± 0.10)	0.207 (± 0.005)	1.968 (± 0.001)	103.33 (± 2.0)	$(\text{MnO}_2)_{0.9364} \cdot (\text{MnOOH})_{0.0635} \cdot 0.207\text{H}_2\text{O}$

Data are presented as the mean (\pm SE; standard error at the 95% level of confidence)

where w is the percentage of the combined water in the sample calculated from the weight loss the occurred during TG between the temperatures 100 and 300 °C. Simultaneously, from Brenet’s values, the cation vacancy fraction x , which represents Ruetschi’s Mn^{4+} vacancies, was calculated (Table 3).

The Ruetschi’s cation vacancy model [24], to explain the physical and electrochemical properties of γ - and ϵ -manganese dioxides, can be summarized as follows. The general formulae of active manganese dioxides, i.e., $(MnO_2)_{2n-3} \cdot (MnOOH)_{4-2n} \cdot mH_2O$ can be represented by:



where x is the fraction of Mn^{4+} missing from the MnO_2 lattice resulting in Mn vacancies and y is the fraction of Mn^{4+} replaced by Mn^{3+} . The parameters x and y in the above equation are related to the Brenet’s parameters n and m . The relation between Brenet’s formula and Ruetschi’s formula are as follows:

$$x = m / (2 + m), \quad (7)$$

$$y = 4 \times (2 - n) / (2 + m) \quad (8)$$

and

$$n = 4(1 - x) - y / 2(1 - x), \quad (9)$$

$$m = 2x / (1 - x). \quad (10)$$

For the samples prepared in present work, the vacancy fraction value varies from 0.061 to 0.093 in ORE-40 to ORE-RT, respectively (Table 3). Consequently, the y value of Ruetschi, which represents Mn^{3+} in MnO_2 , is found to vary between 0.026 and 0.070 in the case of ORE-RT and ORE-40, respectively.

The density was calculated using the relationship:

$$d = 54.94(1 - x) + 32 + 1.008(4x) / V_0 \quad (11)$$

where V_0 is the unit cell volume for γ - MnO_2 ($V_0 = 17.805 \text{ cm}^3$). Introduction of vacancies into the Mn^{4+} sublattice and associated substitutions of four O^{2-} by four OH^- does not lead to a noticeable change in lattice parameters. However, due to the loss of Mn^{4+} ions, the density decreases with increasing vacancy fraction. As per the model, density decreased with the increase in vacancy fraction (Table 3).

The total structural water content was estimated by the formula:

$$\%H_2O = 100 \times 18.016(4x + y) / 2MW \quad (12)$$

where MW is the molecular weight calculated using Eq. 6. The structural water content (in percent) for $y=0$ and $y=0.1$

Table 3 Correlation of physical and electrochemical properties of prepared manganese dioxides

Sample code	x (Ruetschi)	y (Ruetschi)	Molecular weight (g)	Density (g/cm ³)	% H ₂ O for $y=0$ (Ruetschi)	C_w (Ah/g)	C_w (%)	Formula $Mn_{(1-x-y)}^{4+} Mn_y^{3+} O_{(2-4x-y)}^{2-} \cdot OH_{(4x+y)}^{1-}$
ORE-RT	0.093 (± 0.001)	0.026 (± 0.003)	82.30 (± 0.06)	4.622 (± 0.003)	3.994 (± 0.053)	0.287 (± 0.001)	93.34 (± 0.33)	$Mn_{0.888}^{4+} Mn_{0.026}^{3+} O_{1.608}^{2-} \cdot OH_{0.391}^{1-}$
ORE-40	0.061 (± 0.003)	0.066 (± 0.007)	83.85 (± 0.15)	4.705 (± 0.008)	2.659 (± 0.138)	0.277 (± 0.002)	90.84 (± 0.85)	$Mn_{0.870}^{4+} Mn_{0.007}^{3+} O_{1.683}^{2-} \cdot OH_{0.316}^{1-}$
ORE-60	0.086 (± 0.003)	0.056 (± 0.002)	82.58 (± 0.18)	4.635 (± 0.010)	3.777 (± 0.169)	0.278 (± 0.001)	90.40 (± 0.16)	$Mn_{0.856}^{4+} Mn_{0.055}^{3+} O_{1.603}^{2-} \cdot OH_{0.396}^{1-}$
ORE-80	0.091 (± 0.002)	0.061 (± 0.002)	82.20 (± 0.10)	4.614 (± 0.005)	4.111 (± 0.096)	0.276 (± 0.001)	89.82 (± 0.29)	$Mn_{0.848}^{4+} Mn_{0.057}^{3+} O_{1.575}^{2-} \cdot OH_{0.424}^{1-}$

Data are presented as the mean (\pm SE); standard error at the 95% level of confidence

is plotted as a function of cation vacancy x in Fig. 6. The values obtained are in agreement with those calculated from TG data. As predicted, the increase in cation vacancy led to increased structural water content.

The theoretical (maximum) electrochemical capacity deliverable per unit weight (C_w) was calculated as follows [24]:

$$C_w = (1 - x - y) \times 26.8/MW \quad (13)$$

where 26.8 is the theoretical mAh [33]. From C_w values, the percentage theoretical electrochemical capacity ($\%C_w$) was calculated using the relation:

$$\%C_w = 100 \times C_w/0.308 \quad (14)$$

where 0.308 is the theoretical output of pure MnO_2 [34] (note: $x=0$ and $y=0$ for pure MnO_2). The $\%C_w$ was found to decrease with increasing vacancy fraction and with increasing water content (Table 3). Thus, a high percentage of structural water is undesirable as regards to capacity. However, a certain amount of it is necessary for a fast proton transfer rate, which is responsible for electrochemical activity [24].

Electrochemical activity

Figures 7 and 8 presents the discharge curves in 9 M KOH at 1 mA/0.1 g and 100 Ω /0.5 g, respectively. The amount of energy obtained from any MnO_2 depends on the origin and method of preparation. Electrochemically, quantity generated on constant load to a certain end-voltage determines relative activity. It not only depends on the quality of MnO_2 , but also on the structural and dimensional features of the cathode. The latter is due to two kinds of diffusion processes. First is diffusion within the particle of MnO_2 ; solid-state diffusion depending on the physical and chemical properties of MnO_2 . In this context, differences in electrochemical reactivity of manganese dioxides can be easily recognized by discharging them in 9 M KOH

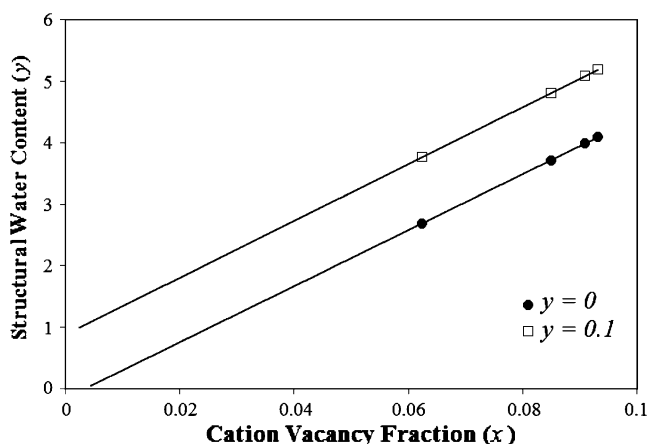


Fig. 6 Structural water content (y) as a function of Mn^{4+} vacancy fraction (x)

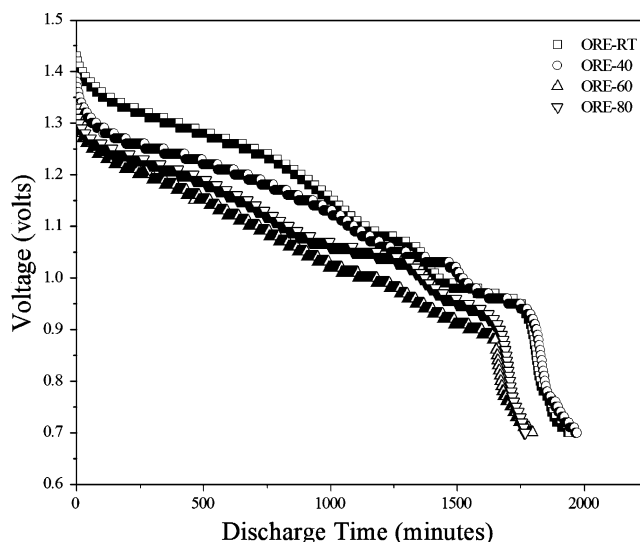


Fig. 7 Discharge curves of prepared samples in 9 M KOH at constant current (1 mA)

solution. Since this method has added advantage of supposedly being independent of cell fabrication factors [35], it has been adopted in the present work.

For low and medium discharge rates, electrochemical reduction of MnO_2 occurs in two steps. The first step is from $MnO_2 \rightarrow MnO_{1.5}$. This phase is regarded as homogeneous phase reduction [10, 36], represented by the following equation:



As the discharge proceeds, the concentration of Mn^{3+} and OH^- ions increases gradually and finally MnO_2 is converted to $MnOOH$. Both protons and electrons move

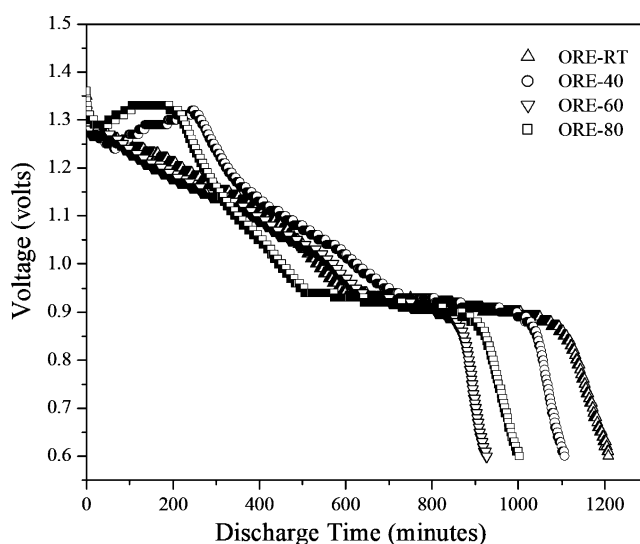


Fig. 8 Discharge curves of prepared samples in 9 M KOH at constant resistance (100 Ω)

Table 4 Discharge characteristics of MnO₂ samples in 9 M KOH at constant current 1 mA/0.1 g

Sample code	Open circuit voltage (V)	Discharge time to 0.9 V cutoff (min)	Discharge capacity 0.9 V cutoff (mA h/0.1 g)	Percent utilization against theoretical capacity	Gravimetric energy density ^a (W h/kg)	Volumetric energy density ^a (W h/L)
ORE-RT	1.449 (±0.001)	1,795 (±2.0)	29.93 (±0.03)	97.17 (±0.10)	88.07 (±0.09)	216.96 (±0.23)
ORE-40	1.425 (±0.004)	1,813 (±2.9)	30.23 (±0.04)	98.14 (±0.16)	86.43 (±0.12)	212.91 (±0.31)
ORE-60	1.396 (±0.004)	1,595 (±2.6)	26.58 (±0.04)	86.29 (±0.14)	75.21 (±0.10)	185.28 (±0.26)
ORE-80	1.397 (±0.009)	1,668 (±2.0)	27.81 (±0.03)	90.29 (±0.10)	76.82 (±0.08)	189.24 (±0.21)

All calculations for 100 mg MnO₂ sample. Data are presented as the mean (±SE; standard error at the 95% level of confidence)

^a Cutoff is 0.7 V, based on the obtained average operating voltage per cell

freely within the MnO₂ lattice during the electrochemical reduction. As a result, the potential decreases and produces an S-shaped curve [37]. The reaction can be described as one wherein one solid structure (MnO₂) gets converted to another (MnOOH) without changing its basic structure. The useful capacity of ordinary alkaline manganese dioxide cells on the market today lies within this step of discharge [13]. The second step of the reaction (MnO_{1.5}→MnO_{1.0}) consists of the reduction of MnOOH→Mn(OH)₂ via dissolution and precipitation processes. It is regarded as heterogeneous phase reduction, and the potential during this stage remains almost constant over the major portion of the step. It is observed (Fig. 7) that the prepared samples showed long discharge plateaus indicating high activity, which practically corresponds to high quantity of electricity involved in the electrochemical reaction. The energy output in terms of gravimetric and volumetric energy density (Tables 4 and 5) and percent utilization of MnO₂ material against theoretical capacity (Table 4) suggests that the samples prepared in the present work show high electrochemical activity.

The value of electrochemical activity ultimately depends upon how effectively reaction 15 takes place. In other words, the rate at which protons are transferred to undischarged Mn⁴⁺ ions decides the activity. The protons are present in the form of OH⁻ ions into the MnO₂ lattice as a consequence of Mn⁴⁺ cation vacancies. These OH⁻ ions act as proton donors, thereby, providing the initial concentration of protons to carry out reaction 15. The probability

of proton transfer from Mn vacancy to undischarged Mn⁴⁺ is expressed as [24]:

$$P_t = \nu[\text{OH}^-][\text{O}^{2-}] \tag{16}$$

where ν is the jump frequency, [OH⁻] represents concentration of proton occupied sites, and [O²⁻] represents the concentrations of available, suitable empty sites for proton transfer. If these concentration terms are expressed as the number of ions per molecular volume, i.e., in terms of Ruetschi’s model, Eq. 16 becomes:

$$P_t = \nu(4x + y)(2 - 4x - y). \tag{17}$$

In γ -MnO₂, two types of [O²⁻] and [OH⁻] sites are present: the planar [O²⁻], [OH⁻]_{pl}, and the pyramidal [O²⁻], [OH⁻]_p, configuration with respect to the three next-neighboring Mn⁴⁺ ions. Only the “pyramidal” O²⁻ is suitable for proton uptake [38]. According to that reported by Reutschi [24], the rate of proton transfer (P_t) in γ -MnO₂ could thus be visualized as being proportional to:

$$P_t = [\text{OH}^-]_{\text{pl}} \times [\text{OH}^-]_{\text{p}} \times [\text{O}^{2-}]_{\text{p}} \tag{18}$$

$$= (4 - p)x \times (px + y) \times (1 - px - y)$$

where p denotes OH⁻ ions occupying pyramidal sites and its value can be 1, 2, or 3 depending upon the special distribution of four OH⁻ ions around a vacancy. This expression is plotted in Fig. 9 as a function of x , for $p=2$, and for several values of y as parameter. According to the Ruetschi’s model, for small values of x , the rate of proton

Table 5 Discharge characteristics of MnO₂ samples in 9 M KOH at constant resistance 100 Ω/0.5 g

Sample code	Open circuit voltage (V)	Discharge time to 0.6 V cutoff (min)	Discharge capacity ^a (mA h/0.5 g)	Gravimetric energy density ^a (W h/kg)	Volumetric energy density ^a (W h/L)
ORE-RT	1.424 (±0.005)	1,208 (±1.7)	201.73 (±0.29)	97.78 (±0.14)	240.88 (±0.34)
ORE-40	1.430 (±0.005)	1,106 (±3.1)	194.22 (±0.55)	98.50 (±0.28)	242.66 (±0.69)
ORE-60	1.434 (±0.007)	924 (±4.1)	160.12 (±0.41)	80.44 (±0.20)	198.17 (±0.51)
ORE-80	1.446 (±0.002)	1,003 (±2.3)	172.51 (±0.39)	85.84 (±0.19)	211.47 (±0.48)

All calculations for 500 mg MnO₂ sample. Data are presented as the mean (±SE; standard error at the 95% level of confidence)

^a Cutoff is 0.6 V, based on obtained average operating voltage per cell

transfer increases with the cation vacancy fraction (x) and OH^- concentration, i.e., structural water content. It reaches maximum at $x=0.25$ and thereafter decreases. Hence, the electrochemical activity of prepared samples should also increase with x , till x reaches 0.25 and decrease thereafter.

The values of x for the samples prepared in the present work are in the range $0.062 < x < 0.093$, i.e., within the specified range ($x < 0.25$). The energy density varies linearly with x (Tables 3 and 4), implying that the electrochemical activity of the prepared samples is directly proportional to the cation vacancy fraction (x) and OH^- concentration. The cation vacancy of the prepared samples increases in order $\text{ORE-40} < \text{ORE-60} < \text{ORE-80} < \text{ORE-RT}$. Thus, ORE-RT with maximum x value (Table 3) shows maximum energy density (Table 4). It is also worth mentioning that the corresponding y value is lowest in the case of ORE-RT. The y value, which signifies Mn^{3+} content in the sample [24], can result in decreased electrochemical performance due to the formation of inactive Mn(III) intermediate. This is clearly reflected in case of samples ORE-80 and ORE-60, which, despite having reasonably high x value, show decrease in energy density owing to high content of Mn^{3+} ions (y). ORE-40 with in-between x and y values show moderate electrochemical performance. Thus, the cation vacancy fraction (x) and OH^- concentration (structural water content) and Mn^{3+} content (y) determines the electrochemical activity for the prepared samples.

Cyclic voltammetry

Figure 10 shows the cyclic voltammogram of ORE-RT in potential range 400 to -800 mV for the first four cycles. The values of reduction and oxidation peaks for first four scans have been given in Table 6. The homogeneous phase reduction shown by Eq. 15 takes place in the region 200 to -300 mV. The peak at -220 mV signifies the formation of MnOOH , i.e., Mn(III) species (process V^1) through

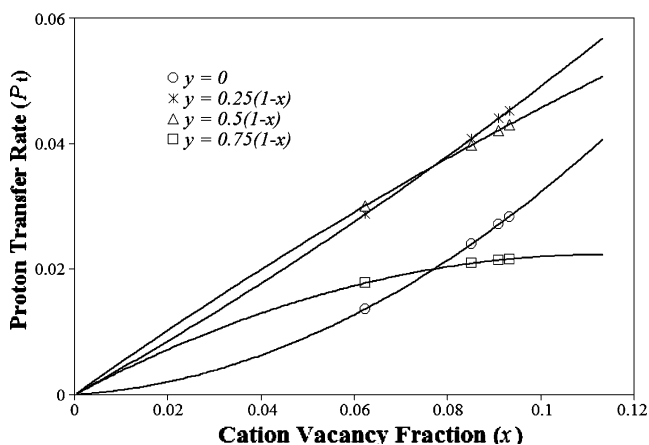


Fig. 9 Proton transfer rate (P_t) as a function of Mn^{4+} vacancy fraction (x)

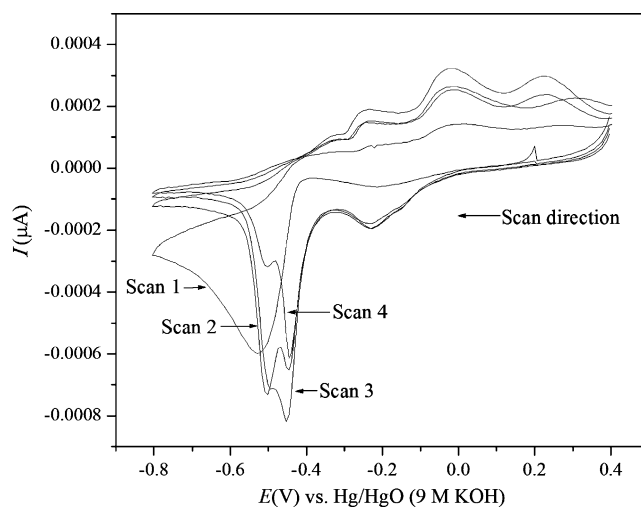
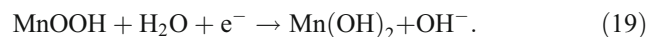


Fig. 10 Cyclic voltammogram of ORE-RT in 9 M KOH. Reference electrode, $\text{Hg}/\text{HgO}/9$ M KOH; scan rate, 2 mV/s

simultaneous intake on protons and electrons during the reduction [39, 40]. A well-defined peak at around -500 mV is due to the heterogeneous reduction of $\text{MnOOH} \rightarrow \text{Mn}(\text{OH})_2$ via dissolution–precipitation mechanisms (process V^2) according to reaction 19 [39–41]:



The corresponding oxidation in the voltammogram is observed by anodic peaks at -230 mV (process V^4) and -10 mV (process V^5) indicating regeneration of Mn(III) species [15, 40–42]. As a consequence, the behavior observed during the subsequent discharge is different and results in a lower capacity [43, 44].

For the subsequent voltammetric cycles, cathodic reduction peak due to the formation of $\text{Mn}(\text{OH})_2$ is shifted near -450 mV. This decrease in overpotential is attributed to larger quantities of Mn^{3+} formed during the first cycle [15, 44]. The presence of an additional shoulder-like peak at -500 mV (process V^3) is attributed to the formation of Mn_3O_4 [15, 40]. During reverse sweep, formation of Mn

Table 6 Voltammetric data of ORE-RT in 9 M KOH for different scans

Process	Scan 1 (mV)	Scan 2 (mV)	Scan 3 (mV)	Scan 4 (mV)
V^1	-210	-220	-220	-220
V^2	-520	-450	-450	-440
V^3	–	-500	-490	-500
V^4	-230	-230	-240	-230
V^5	-10	-10	-10	-10
V^6	310	230	230	250

(III) species and finally to δ -MnO₂ (process V⁶) is attributed to electrochemical processes taking place due to anodic oxidation of Mn(OH)₂ [40, 41]. The sharpness of peaks in the voltammogram indicates a fast charge transfer facilitated by highly accessible pore structure in which the diffusion of ions is rapid and unhindered [45]. The lower peak separation signifies an increase in the reversibility of the electrochemical redox processes. During voltammetric cycles, if the formation of Mn(OH)₂ is avoided, i.e., by cycling in the region 400 to –300 mV, the MnO₂ electrode can be used for more charge–discharge cycles [40, 46].

Conclusions

γ -MnO₂ with high purity, surface area, and electrochemical activity was synthesized starting from Nagpur-based manganese ore. Structural investigations showed the formation of the hcp oxygen sublattice where Mn⁴⁺ cation vacancies of the octahedral positions. The heavy microtwinning ($T_w > 70\%$) observed was due to the merging of peaks 221/240 and 061/002 of original orthorhombic symmetry. Mn⁴⁺ vacancy for charge compensation coordinated with protons, which are present in the MnO₂ lattice in the form of OH[–] ions. The OH[–], which coordinated with Mn⁴⁺ vacancy, supplies protons necessary to carry out the discharge process. The discharge process in 9 M KOH was found to be governed by the solid-state proton diffusion process, wherein Mn⁴⁺ and Mn³⁺ coexisted producing an S-shaped curve. The rate of proton transfer (P_t) during the reaction increased with increasing vacancy fraction, as suggested by Ruetschi's model. The cation vacancy fraction (x), OH[–] concentration (structural water content), and Mn³⁺ content (y) influenced the electrochemical activity of the prepared samples. Cyclic voltammetry detected the presence of Mn(III) and Mn(II) species in the potential range 200 to –350 and –350 to –800 mV, respectively, during the reduction cycle. During oxidation, cycle regeneration of Mn(III) species is observed in the potential range –300 to 0 mV, while formation of δ -MnO₂ is detected at ~230 mV.

References

- Pagnanelli F, Sambenedetto C, Furlani G, Veglio F, Toro L (2007) J Power Sources 166:567. doi:10.1016/j.jpowsour.2007.01.066
- Manickam M (2008) J Electroanal Chem 616:99. doi:10.1016/j.jelechem.2008.01.011
- Sharma MM, Krishnan B, Zachariah S, Shah CU (1999) J Power Sources 79:69. doi:10.1016/S0378-7753(99)00045-2
- Zhang W, Cheng CY (2007) Hydrometallurgy 89:137. doi:10.1016/j.hydromet.2007.08.010
- Abou-El-Sherbini KS (2002) Sep Purif Technol 27:67. doi:10.1016/S1383-5866(01)00193-9
- Darmane Y, Cherkaoui M, Kitane S, Alaoui A, Sebban A, Touhami ME (2008) Hydrometallurgy 92:73. doi:10.1016/j.hydromet.2008.01.007
- Atlam A (1997) Hydrometallurgical treatment of Egyptian low-grade manganese ore. Metall (Heidelberg) 51:486
- Fernandes JB, Desai BD, Dalal VNK (1985) J Power Sources 15:209. doi:10.1016/0378-7753(85)80075-6
- Fernandes JB, Desai BD (1991) J Power Sources 34:207. doi:10.1016/0378-7753(91)80088-F
- Abbas H, Abou-El-Sherbini KS, Askar M, Hashem AM (2001) J Mar Sci Technol 17:351
- Hashem AM, Abou-El-Sherbini KS, Zein-El-Abedin S, Abbas H (2006) J Mar Sci Technol 22:25
- Kozawa A (1974) In: Kordesch K (ed) Batteries, vol 1, manganese dioxide. Marcel Dekker, New York, p 442
- Vogel AI (1989) A textbook of quantitative inorganic analysis, 5th edn. Addison Wesley Longmans, London, p 336
- Indian Standard (1996) Manganese dioxide for dry batteries, IS-11153
- Fiedler DA (1998) J Solid State Electrochem 2:315. doi:10.1007/s100080050106
- Malpas DG, Tye FL In: Glover D, Schumm Jr B, Kozawa A (eds) Handbook of manganese dioxides, battery grade, chapter V. IBA Inc & JEC Press Inc, Brunswick
- Chabre Y, Pannetier J (1995) Prog Solid State Chem 23:1. doi:10.1016/0079-6786(94)00005-2
- De Wolff PM, Visser JW, Giovanoli R, Brutsch R (1978) Chimia (Aarau) 32:257
- Simon DE, Morton RW, Gislason JJ (2004) Adv X-ray Anal 47:267
- Chang-Hoon K, Zentaro A, Lichun Z, Heuer AH, Newman AE, Hughes PJ (2006) J Solid State Chem 179:753. doi:10.1016/j.jssc.2005.11.042
- Abbas H, Nasser SA (1996) J Power Sources 58:15. doi:10.1016/0378-7753(95)02770-X
- Fernandes JB, Desai BD, Dalal VNK (1985) Electrochim Acta 28:309. doi:10.1016/0013-4686(83)85127-5
- Ananth MV, Pethkar S, Dakshinamurthi K (1998) J Power Sources 75:278. doi:10.1016/S0378-7753(98)00100-1
- Ruetschi P (1984) J Electrochem Soc 131:2737. doi:10.1149/1.2115399
- Lee JA, Newnham CE, Stone FS, Tye FL (1973) J Colloid Interface Sci 45:289. doi:10.1016/0021-9797(73)90269-5
- Brenet JP, Faber P (1995) Symp. I.S.E. Batteries Marcoussis, France
- Sharp JH, Tinsley DM (1971) J Therm Anal 3:43. doi:10.1007/BF01911769
- Fernandes JB, Desai BD, Dalal VNK (1985) J Power Sources 16:1. doi:10.1016/0378-7753(85)80001-X
- Liu B, Thomas PS, Ray AS, Williams RP (2004) J Therm Anal Calorim 76:115. doi:10.1023/B:JTAN.0000027810.56753.0d
- Zaki MI, Hasan MA, Pasupulety L, Kumari K (1997) Thermochem Acta 303:171. doi:10.1016/S0040-6031(97)00258-X
- Gonzalez C, Gutierrez JI, Gonzales-Velasco JR, Cid A, Arranz A, Arranz JF (1998) J Therm Anal Calorim 52:985. doi:10.1023/A:1010132606114
- Brenet JP, Cyrankowska M, Ritzler G, Saka R, Traore K (1975) Proceedings of the MnO₂ Symposium, Cleveland, OH, USA, 1:276
- Desai BD, Dhume RAS, Dalal VNK (1988) J Appl Electrochem 18:62. doi:10.1007/BF01016206
- Bell GS, Bauer J (1969) Electrochim Acta 14:453. doi:10.1016/0013-4686(69)87030-1
- Kozawa A (1979) Prog Batteries Sol Cells 2:104
- Scott AB (1960) J Electrochem Soc 107:941. doi:10.1149/1.2427575
- Kozawa A, Powers RA (1966) J Electrochem Soc 113:570
- Maskell WC, Shaw IE, Tye FL (1983) Electrochim Acta 28:225. doi:10.1016/0013-4686(83)85113-5

39. Kozawa A (1974) In: Kordesch K (ed) 'Batteries', volume I, manganese dioxide. Marcel Dekker, New York, p 385
40. McBreen J (1975) *Electrochim Acta* 20:221. doi:[10.1016/0013-4686\(75\)85028-6](https://doi.org/10.1016/0013-4686(75)85028-6)
41. Fiedler DA, Besenhard JO, Fooker MH (1997) *J Power Sources* 69:157. doi:[10.1016/S0378-7753\(97\)02513-5](https://doi.org/10.1016/S0378-7753(97)02513-5)
42. Ghaemi M, Gholami A, Moghaddam RB (2008) *Electrochim Acta* 53:3250. doi:[10.1016/j.electacta.2007.10.015](https://doi.org/10.1016/j.electacta.2007.10.015)
43. Ghaemi M, Khosravi-Fard L, Neshati J (2005) *J Power Sources* 141:340. doi:[10.1016/j.jpowsour.2004.10.004](https://doi.org/10.1016/j.jpowsour.2004.10.004)
44. Jouanneau S, Le Gal La Salle A, Guyomard D (2002) *Electrochim Acta* 48:11. doi:[10.1016/S0013-4686\(02\)00485-1](https://doi.org/10.1016/S0013-4686(02)00485-1)
45. Bertel E, Memmel N (1996) *Appl Phys A* 63:523. doi:[10.1007/BF01567208](https://doi.org/10.1007/BF01567208)
46. Boden D, Venuto CJ, Wisler D, Wylie RB (1968) *J Electrochem Soc* 115:33. doi:[10.1149/1.2410996](https://doi.org/10.1149/1.2410996)